

UNIVERSAL MEDICAL IMAGING MODEL FOR DOMAIN GENERALIZATION WITH DATA PRIVACY

Ahmed Radwan, Islam Osman, Mohamed S. Shehata

University of British Columbia
Department of Computer Science
3333 University Way, Kelowna, BC

ABSTRACT

Achieving domain generalization in medical imaging poses a significant challenge, primarily due to the limited availability of publicly labeled datasets in this domain. This limitation arises from concerns related to data privacy and the necessity for medical expertise to accurately label the data. In this paper, we propose a federated learning approach to transfer knowledge from multiple local models to a global model, eliminating the need for direct access to the local datasets used to train each model. The primary objective is to train a global model capable of performing a wide variety of medical imaging tasks. This is done while ensuring the confidentiality of the private datasets utilized during the training of these models. To validate the effectiveness of our approach, extensive experiments were conducted on eight datasets, each corresponding to a different medical imaging application. The client's data distribution in our experiments varies significantly as they originate from diverse domains. Despite this variation, we demonstrate a statistically significant improvement over a state-of-the-art baseline utilizing masked image modeling over a diverse pre-training dataset that spans different body parts and scanning types. This improvement is achieved by curating information learned from clients without accessing any labeled dataset on the server.

Index Terms— Domain Generalization, Medical Imaging, Deep Learning, Data Privacy, Federated Learning

1. INTRODUCTION

In the past decade, the field of machine learning (ML), particularly deep learning (DL), has witnessed significant advancements, paving the way for successful applications across various domains. Healthcare stands out as a field with immense potential for transformation due to these DL breakthroughs. The application of DL in healthcare not only holds the promise of directly impacting human life but also offers the potential to alleviate the burden on medical professionals and reduce diagnostic errors. Despite the remarkable achievements of DL techniques in healthcare, three primary challenges demand attention.

Firstly, the success of DL often relies on scaling models to incorporate billions of parameters, necessitating the use of massive datasets. While datasets are typically present on the same machine as the model during training, the practical scenario involves the collection of datasets from various locations. These datasets are then aggregated and transmitted to a central server for model training, introducing communication overhead, particularly when dealing with massive datasets.

Secondly, the healthcare domain presents an added layer of complexity due to the stringent protection of personal health information (PHI) by regulatory laws such as HIPAA and PIPEDA. Safeguarding patient data privacy is a critical consideration in the development and deployment of machine learning models in healthcare.

Finally, ML applications in healthcare are diverse, and they usually involve different types of image scanning techniques. This introduces huge domain shifts and requires models specializing in each domain to achieve good performance, which demands a lot of resources. Moreover, isolated models cannot leverage the commonalities that may exist across these tasks, which can be used to improve the performance across all the tasks. Additionally, it is common to have models that work well on a specific dataset but fail to generalize well when a significant domain shift is present. This can particularly raise concerns regarding the trustworthiness of the model, especially when the model decisions can be critical to decision-making regarding patients' health.

In this paper, we propose a novel method dubbed MedUniverse to address the aforementioned challenges. Our contributions can be summarized as follows:

- We collect diverse datasets that span most medical image classification applications to train and test the domain generalization capabilities of our framework.
- We utilize a federated learning framework for constructing our MedUniverse model, where each client can protect the privacy of their datasets while allowing the server's model to learn from the finetuned client weights
- We achieve strong performance on a variety of tasks

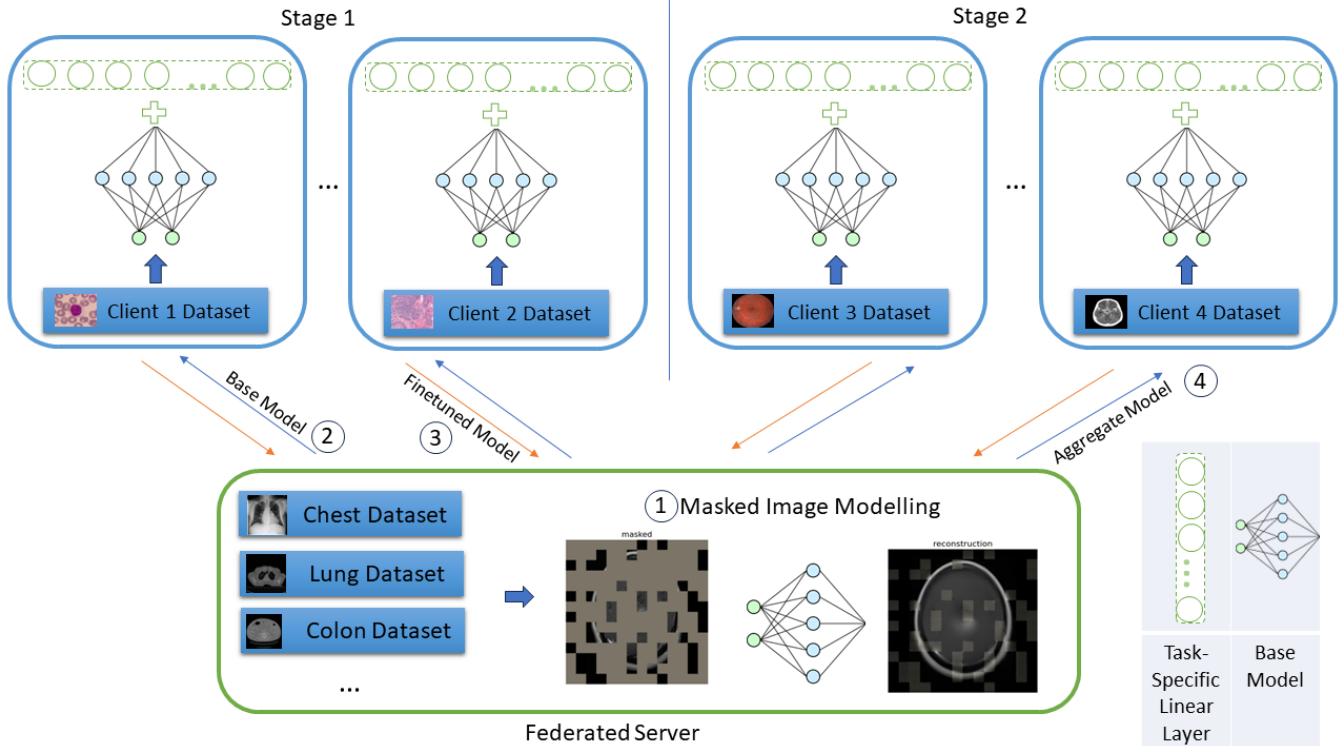


Fig. 1: The figure illustrates our Stage-wise federated learning pipeline. 1) The server initializes its base model via self-supervised MIM on data spanning different parts of the human body obtained via different scanning techniques to maintain domain diversity. 2) Clients query the server with the number of classes in their classification problem, and the server sends its base model followed by a randomly initialized linear layer. 3) The client fine-tunes the base model and sends the fine-tuned model back to the server. After receiving a pre-determined number of clients’ fine-tuned models, the server concludes the stage, aggregates the weights, and updates the base model as explained in the methodology. 4) The server then sends the updated model to the clients in the next stage.

where a significant domain shift exists, moreover we show improvements across all tasks even when the domains strongly vary.

2. BACKGROUND & RELATED WORK

2.1. Domain Generalization

Standard machine learning approaches can demonstrate formidable performance on specific tasks by splitting the dataset and training on a subset. This assumes that the training and testing data are Independent and identically distributed (i.i.d). However, this is rarely the case with any real-life problem since the testing data distribution can shift over time due to many considerations. In the medical domain, this can prevail in the form of hardware degradation, changes in the scanner hardware, or a different distribution of patients. The domain shift issue is even more prevalent when we completely switch to a different domain, and it usually leads to a huge drop in performance, as shown in work like [1]. The task of domain generalization can be considered as

a form of transfer learning, where we would like to have a model that can generalize to distributions unseen at the test time. The term was first introduced in [2], where a Domain-Invariant Component Analysis approach was introduced to learn a transformation of the data that minimizes the dissimilarities across the different domains while maintaining a valid input-output mapping through the model.

2.2. Masked Image Modelling

The common scheme in domain generalization is learning domain invariant representations that can be generalized to multiple domains. The idea of masked modeling was first applied in the field of Natural Language Processing (NLP) [3] to train transformers in a self-supervised manner. Inspired by this success, [4] applies the same technique in computer vision. In Masked Image Modelling (MIM), the image is divided into a set of patches, where a subset is randomly masked out, and the network is trained to reconstruct the hidden patches. The paper first analyzes the key differences between the visual and linguistic input, then proposes an encoder-decoder architec-

ture with a bigger masking ratio for the input image patches to solve this task. The MIM can serve as a pretext task, where the pre-trained encoder can be further used in discriminative tasks. In this paper, we also make use of MIM to learn representations from different datasets.

2.3. Federated Learning

Although MIM can successfully learn to model a target domain without access to labeled examples, it still requires access to the unlabelled examples, and in the healthcare domain, this poses a privacy concern where in many cases, it is desired to keep the patients’ data confidential. Moreover, since we have a diverse set of medical image classification tasks, we are going to deal with a lot of datasets, and moving all the data to the model will pose a huge communication overhead. Federated learning is a machine learning paradigm in which an algorithm is trained collaboratively via independent clients, each using their data. A centralized server is responsible for training an initial model and sending to clients upon request. Each client can train the model locally and only send model updates back to the server. The server can then aggregate updates from different clients and update its base model.

3. PROPOSED METHOD

3.1. Base Model

The server utilizes a Vision transformer (ViT) as the backbone for the base model. The model is trained in a self-supervised way using masked image modeling.

3.2. Masked Image Modelling

We utilize masked image modeling to pre-train the base model. Following the footsteps of [4], the input image is first divided into patches, the patches are split into two non-overlapping sets of visible, and hidden patches. The ViT-based encoder is fed with the visible patches, to which positional encoding is added as done with the standard vision transformer. The visible patches that the encoder works with are only around 25% of the number of patches. This ensures that the model cannot leverage the redundancy present in most images and helps it learn the actual underlying distribution of the image. Finally, the encoder outputs a set of encoded visible patches which will be later processed by the decoder.

The decoder receives a set of encoded visible patches and mask tokens, where mask tokens are learnable and indicate the presence of a masked-out patch. Positional encoding is applied to all input tokens, and the decoder is tasked with reconstructing the pixel values of the masked patches.

3.3. Stage-Wise Federated Learning

After pre-training the base model via MIM, the server sends the base model Z_b to a requesting client C_i that aims to solve a medical image classification task with N_i classes and M_i training examples. The server appends a linear, fully connected layer to the base model and sends it to the client for fine-tuning. The client C_i sends the model weights Z_i back to the server. The server, after receiving K client updates, declares a stage has ended and aggregates the received model updates via a weighted average with the formula:

$$\hat{Z}_b = \frac{1}{\sum_i^K M_i} \sum_i^{1:K} Z_i \times M_i \quad (1)$$

This allows the base model updates to not be dominated by clients who have few labeled examples. The updated model will be sent to the client in the next stages, will be the base for the fine-tuning done by the clients, and will eventually get sent back to the server. This effectively allows the server to keep a rolling update of its base parameters over time.

3.4. Data Privacy

Since each client reports back to the server the fine-tuned weights of the base model (as well as the number of training examples), the client maintains the privacy of their data points. Moreover, the client doesn’t need to send the final linear classification layer either, further maintaining privacy by hiding the direct statistical correlation between the features and the final output.

3.5. Model Trustworthiness

To ensure that the server model doesn’t diverge, a paired samples t-test will be conducted after every S stage. The null hypothesis is that the means of the experiment and control populations are equal $H_0 : \mu_1 = \mu_2$. The alternative hypothesis (two-tailed) is that the two population means are not equal and is given by $H_1 : \mu_1 \neq \mu_2$. The test statistic t is given by the formula:

$$t = \frac{\bar{x}_d}{s_d/\sqrt{n}} \quad (2)$$

Where \bar{x}_d is the sample mean of the differences, s_d is the sample standard deviation of the differences, and n is the sample size. We also calculate the effect size for our t-test using Cohen’s d measure. The d statistic is given by the formula:

$$Cohen's\ d = \frac{|\bar{x}_d|}{s_d} \quad (3)$$

The effect size calculation will be used to report if the difference is big enough since the results could be statistically significant but trivial. If the updated server model \hat{Z}_b brings

Body Part	Dataset	Scan Type
Chest	NIH Chest XRay [6]	X-Ray
	RIDER Lung CT [7], [8]	CT
	LIDC-IDRI [9], [8]	CT / CR / DX
Lung	COVID-19-NY-SBU [10],[8]	CR / CT / DX / MR / PT / NM / OT / SR
	COVID-19 CT [11], [8]	CT
	MIDR-RICORD-1a & 1b [12], [8]	CT
	QIN Lung CT [13], [8]	CT
	LungCT-Diagnosis [14], [8]	CT
	NSCLC-Radiomics-Genomics [15], [8]	CT
	COVID-19-AR [16], [8]	CT / DX / CR
	CMB-LCA [17], [8]	CT / DX / MR / NM / US
Pancreas	Ctpred-Sunitinib-panNet [18], [8]	CT
	Pancreas CT [19], [8]	CT
Colon	CT COLON ACRIN 6664 [20], [8]	CT
	CMB-CRC [21], [8]	CT / DX / MR / PT / US
Bladder	TCGA-BLCA [22], [8]	CT / CR / MR / PT / DX / Pathology
Uterus	TCGA-UCEC [23], [8]	CT / CR / MR / PT / Pathology
Kidney	TCGA-KIRC [24], [8]	CT / MR / CR / Pathology
	CPTAC-CCRCC [25], [8]	CT / MR / Pathology
Prostate	CMB-PCA [26], [8]	CT / MR / NM
Ovary	TCGA-OV [27], [8]	CT / MR / Pathology
Rectum	TCGA-READ [28], [8]	CT / MR / Pathology
	Pseudo-PHI-DICOM-Data [29], [8]	CR / CT / DX / MG / MR / PT
Miscellaneous	Stagell-Colorectal-CT [30], [8]	CT
	CT-ORG [31], [8]	CT
	Pelvic-Reference-Data [32], [8]	CT
	TCGA-SARC [33], [8]	CT / MR / Pathology

Table 1: A breakdown by body parts of the datasets used to pre-train the server’s base model. The dataset images are obtained using different scanning techniques.

both significant and non-trivial improvements as compared to Z_b , it will be retained. If there is no improvement, the base model Z_b will be retained to ensure the trustworthiness of our model performance across not only unseen test data but also across completely different tasks.

4. EXPERIMENTS AND RESULTS

4.1. Pre-training Datasets

In order to achieve domain generalization, our pre-text pre-training task must span a diverse set of medical datasets. Following the footsteps of [5], we utilize a diverse dataset that spans more than 10 different body parts as well as different image scans. Table 1 shows the datasets used for pre-training the server model.

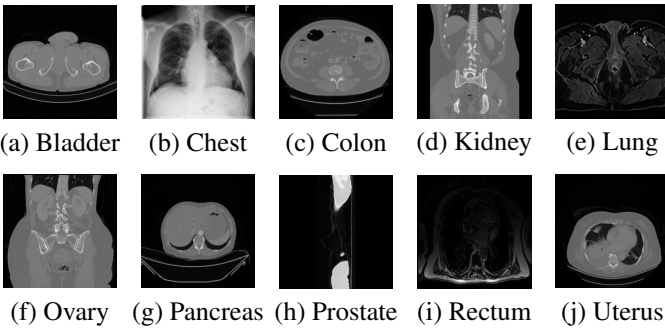


Fig. 2: Samples of the pretraining dataset.

4.2. Stage-wise Federated Learning

We collected 8 additional public datasets that span different medical imaging applications, as well as a huge private dataset. The datasets span different medical applications.

We split the 8 datasets into 4 stages, with 2 clients per stage to be able to test our approach on as many stages as possible. Each stage represents clients that train concurrently. After the training ends, the server gets updated as mentioned in the methodology. To test the efficacy of our model, starting from stage 2, we will repeat all the experiments twice. Once starting from the pre-trained weights of the server (the control group) and once from our updated server model (the test group). The results are presented in table 2

Stage 1 datasets comprise a 1) *brain tumor classification dataset* [34] which has 3264 MRI images. The task is to classify images into three types of different tumors as well as a no-tumor class. 2) *White blood cells 5-class classification dataset* [35]. white blood cells, also known as leukocytes, consist of phagocytes and lymphocytes. Phagocytes act quickly upon infection, while lymphocytes play a role in the acquired immune response. Phagocytes can be further categorized into monocytes, eosinophils, basophils, and neutrophils.

Stage 2 datasets comprise a 1) *Breast Histopathology Images dataset* [36], [37]. The dataset benchmarks the classification of Invasive Ductal Carcinoma (IDC), a common subtype of breast cancer. The dataset comprises 198,738 IDC(-) and 78,786 IDC(+) histopathology image patches. 2) *NCT-CRC-HE-100K* [38] is a dataset comprising 100,000 image patches from H&E stained histological images of human colorectal cancer (CRC) and normal tissue. Each patch is 224x224 pixels with a resolution of 0.5 microns per pixel. The dataset includes nine tissue classes, color-normalized using Macenko’s method [39].

Stage 3 datasets comprise a 1) *COVID-19 Radiography Dataset* [40], [41] is a big collection of X-Ray images which were built on multiple different datasets. This collection comprises COVID-positive (3615), normal (10192 images), Lung Opacity (6012 images), and viral Pneumonia (1345 images). 2) *Breast Ultrasound Images Dataset* [42] comprises breast ultrasound images from women aged 25 to 75, collected in 2018, involving 600 female patients. The dataset contains 780 PNG format images. The images are classified into three categories: normal, benign, and malignant.

Stage 4 datasets comprise a 1) *Ocular Toxoplasmosis Fundus Images dataset* [43] comprises 822 images representing individuals with suspected congenital toxoplasmosis infection. The fundus images are categorized into two main groups, Healthy and Diseased, presenting a binary classification task. 2) *BC Breast Cancer dataset*, which is a private dataset that belongs to the BC Cancer Agency breast cancer chest CT dataset. There are a total of 29,686 patients in this dataset. The dataset contains 57,807 CT series for the patients, taken through the course of the patient’s treatment for

Stage	Dataset	Epochs	Control Accuracy	Experiment Accuracy
Stage 1	brain-tumor-classification-mri	10	80.71%	-
	white-blood-cells	10	98.09%	-
Stage 2	IDC	10	87.66%	88.2%
	NCT-CRC-HE-100k	15	96.18%	96.57%
Stage 3	COVID-19_Radiography_Dataset	50	93.41%	94.23%
	Breast-Ultrasound	100	75.15%	80.89%
Stage 4	ocular-toxoplasmosis-fundus	100	95.18%	100%
	BC Breast Cancer	80	92%	95%

Table 2: The table exhibits the classification accuracies of clients across eight distinct tasks. Clients in the later stages experience greater advantages from the accumulated knowledge accessible at the server, thereby demonstrating a more pronounced performance gap between the experimental and control groups.

breast cancer. Each series contain a range of dice slices, 100 slices per series making it more than 5 million patient scans. The data cohort was collected from the year 1980-2017

4.3. Model Trustworthiness: Paired T-test

We performed a paired sample T-test with a two-tailed distribution (degrees of freedom: 5) after the fourth stage to evaluate the statistical significance of our results compared to the control group. The test was conducted using the common significance level of $\alpha = 0.05$. The paired t-test results indicated a significant and substantial difference between the control group (mean = 89.9, standard deviation = 7.8) and the experimental group (mean = 92.5, standard deviation = 6.9), yielding $t(5) = 2.7$ and $p - value = .044$. As the $p - value$ is less than α , we reject the null hypothesis, indicating that the population average of the experimental group (i.e., the group undergoing fine-tuning with the stage-wise federated approach) is not equal to that of the control group. The observed effect size, represented by d , is large at 1.09, signifying a substantial difference between the average of the observed differences and the expected average of the differences.

5. CONCLUSION

We presented a novel approach to generalize across domains of various medical imaging applications. We showed that our federated approach maintains a model that increases in robustness over time when new clients utilize and finetune the base server model and then send the fine-tuned weights back to the server. While clients in the different stages of our experiment had local data from significantly different domains, they were still able to benefit from the aggregated knowledge from the previous stages.

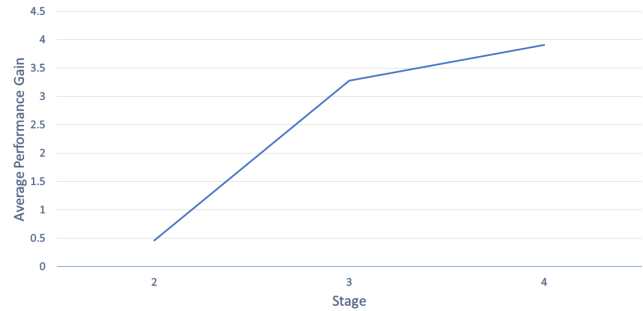


Fig. 3: The plot shows the average accuracy gain across the different stages. As more clients send their fine-tuned weights back to the server, the server can aggregate more knowledge and thus present a more robust model to clients in the next stages.

6. ACKNOWLEDGMENT

The authors acknowledge Isha Shah for validating the approach on the large-scale private BC cancer dataset. The authors also acknowledge 1) the National Cancer Institute and the Foundation for the National Institutes of Health and 2) The Multi-national NIH Consortium for CT AI in COVID-19. 3) the National Cancer Institute’s Cancer Moonshot Biobank, 4) the TCGA Research Network, 5) the National Cancer Institute Clinical Proteomic Tumor Analysis Consortium (CP-TAC) for providing the data which was used as a part of our pre-training dataset

7. REFERENCES

- [1] Reece Walsh, Mohamed H Abdelpakey, Mohamed S Shehata, and Mostafa M Mohamed, “Automated human cell classification in sparse datasets using few-shot learning,” *Scientific Reports*, vol. 12, no. 1, pp. 2924, 2022.
- [2] Krikamol Muandet, David Balduzzi, and Bernhard Schölkopf, “Domain generalization via invariant feature representation,” in *International conference on machine learning*. PMLR, 2013, pp. 10–18.
- [3] Jacob Devlin, Ming-Wei Chang, Kenton Lee, and Kristina Toutanova, “BERT: Pre-training of deep bidirectional transformers for language understanding,” in *Proceedings of the 2019 Conference of the North American Chapter of the Association for Computational Linguistics: Human Language Technologies, Volume 1 (Long and Short Papers)*. June 2019, Association for Computational Linguistics.
- [4] Kaiming He, Xinlei Chen, Saining Xie, Yanghao Li, Piotr Dollár, and Ross Girshick, “Masked autoencoders are scalable vision learners,” in *Proceedings of the*

- IEEE/CVF conference on computer vision and pattern recognition*, 2022, pp. 16000–16009.
- [5] Anuphav Gupta, “Automating computed tomography diagnostic image quality control using deep learning,” M.S. thesis, 2023.
- [6] Xiaosong Wang, Yifan Peng, Le Lu, Zhiyong Lu, Mohammadhadi Bagheri, and Ronald M Summers, “Chestx-ray8: Hospital-scale chest x-ray database and benchmarks on weakly-supervised classification and localization of common thorax diseases,” in *Proceedings of the IEEE conference on computer vision and pattern recognition*, 2017, pp. 2097–2106.
- [7] Binsheng Zhao, Lawrence H Schwartz, and Mark G Kris, “Data from rider_lung ct,” *The Cancer Imaging Archive*, 2015.
- [8] Kenneth Clark, Bruce Vendt, Kirk Smith, John Freymann, Justin Kirby, Paul Koppel, Stephen Moore, Stanley Phillips, David Maffitt, Michael Pringle, et al., “The cancer imaging archive (tcia): maintaining and operating a public information repository,” *Journal of digital imaging*, vol. 26, pp. 1045–1057, 2013.
- [9] SG Armato III, G McLennan, L Bidaut, MF McNitt-Gray, CR Meyer, AP Reeves, B Zhao, DR Aberle, CI Henschke, EA Hoffman, et al., “Data from lidc-idri [data set],” *The Cancer Imaging Archive*, vol. 10, pp. K9, 2015.
- [10] Joel Saltz, Mary Saltz, Prateek Prasanna, Richard Moffitt, Janos Hajagos, Erich Bremer, Joseph Balsamo, and Tahsin Kurc, “Stony brook university covid-19 positive cases [data set]. the cancer imaging archive,” 2021.
- [11] Peng An, Sheng Xu, Stephanie A Harmon, Evrim B Turkbey, Thomas H Sanford, Amel Amalou, Michael Kassin, Nicole Varble, Maxime Blain, Victoria Anderson, et al., “Ct images in covid-19 [data set],” *The Cancer Imaging Archive*, vol. 10, 2020.
- [12] E Tsai, S Simpson, MP Lungren, M Hershman, L Roshkovan, E Colak, BJ Erickson, G Shih, A Stein, J Kalpathy-Cramer, et al., “Medical imaging data resource center (midrc)-rsna international covid-19 open radiology database (ricord) release 1a-chest ct covid+(midrc-ricord-1a),” *The Cancer Imaging Archive*, vol. 202010, 2020.
- [13] J Kalpathy-Cramer, Sandy Napel, D Goldgof, and B Zhao, “Qin multi-site collection of lung ct data with nodule segmentations,” *Cancer Imaging Arch*, vol. 10, pp. K9, 2015.
- [14] Olya Grove, Anders E Berglund, Matthew B Schabath, Hugo JWL Aerts, Andre Dekker, Hua Wang, Emmanuel Rios Velazquez, Philippe Lambin, Yuhua Gu, Yoganand Balagurunathan, et al., “Quantitative computed tomographic descriptors associate tumor shape complexity and intratumor heterogeneity with prognosis in lung adenocarcinoma,” *PloS one*, vol. 10, no. 3, pp. e0118261, 2015.
- [15] HJWL Aerts, E Rios Velazquez, RTH Leijenaar, C Parmar, P Grossmann, S Carvalho, J Bussink, R Monshouwer, B Haibe-Kains, D Rietveld, et al., “Data from nslc-radiomics-genomics. the cancer imaging archive,” 2015.
- [16] S Desai, A Baghal, T Wongsurawat, S Al-Shukri, K Gates, P Farmer, M Rutherford, GD Blake, T Nolan, T Powell, et al., “Data from chest imaging with clinical and genomic correlates representing a rural covid-19 positive population,” *The Cancer Imaging Archive*, 2020.
- [17] Cancer Moonshot Biobank, “Cancer moonshot biobank - lung cancer collection (cmb-lca),” 2022.
- [18] Luohai Chen, Wei Wang, Kaizhou Jin, Bing Yuan, Huangying Tan, Jian Sun, Yu Guo, Yanji Luo, Shi-ting Feng, Xianjun Yu, Min-hu Chen, and Jie Chen, “Prediction of sunitinib efficacy using computed tomography in patients with pancreatic neuroendocrine tumors (ctpred-sunitinib-pannet),” 2022.
- [19] Holger Roth, Amal Farag, Evrim B. Turkbey, Le Lu, Jiamin Liu, and Ronald M. Summers, “Data from pancreas-ct,” 2016.
- [20] Kirk Smith, Kenneth Clark, William C. Bennett, Tracy Nolan, Justin Kirby, Mary Wolfsberger, Joan Moulton, Bruce Vendt, and John Freymann, “Data from ct colonography (acrin 6664),” 2015.
- [21] Cancer Moonshot Biobank, “Cancer moonshot biobank - colorectal cancer collection (cmb-crc),” 2022.
- [22] Shanah Kirk, Yueh Lee, Fabiano R. Lucchesi, Natalia D. Aredes, Nicholas Gruszauskas, James Catto, Kimberly Garcia, Rose Jarosz, Vinay Duddalwar, Bino Varghese, Kimberly Rieger-Christ, and John Lemmerman, “The cancer genome atlas urothelial bladder carcinoma collection (tcga-blca),” 2016.
- [23] Bradley J. Erickson, David Mutch, Lynne Lippmann, and Rose Jarosz, “The cancer genome atlas uterine corpus endometrial carcinoma collection (tcga-ucec),” 2016.
- [24] Oguz Akin, Pierre Elnajjar, Matthew Heller, Rose Jarosz, Bradley J. Erickson, Shanah Kirk, Yueh Lee,

- Marston W. Linehan, Rabindra Gautam, Raghu Vikram, Kimberly M. Garcia, Charles Roche, Ermelinda Bonaccio, and Joe Filippini, "The cancer genome atlas kidney renal clear cell carcinoma collection (tcga-kirc)," 2016.
- [25] National Cancer Institute Clinical Proteomic Tumor Analysis Consortium (CPTAC), "The clinical proteomic tumor analysis consortium clear cell renal cell carcinoma collection (cptac-ccrcc)," 2018.
- [26] Cancer Moonshot Biobank, "Cancer moonshot biobank - prostate cancer collection (cmb-pca)," 2022.
- [27] Chandra Holback, Rose Jarosz, Fred Prior, David G. Mutch, Priya Bhosale, Kimberly Garcia, Yueh Lee, Shanah Kirk, Cheryl A. Sadow, Seth Levine, Evis Sala, Pierre Elnajjar, Tara Morgan, and Bradley J. Erickson, "The cancer genome atlas ovarian cancer collection (tcga-ov)," 2016.
- [28] Shanah Kirk, Yueh Lee, Cheryl A. Sadow, and Seth Levine, "The cancer genome atlas rectum adenocarcinoma collection (tcga-read)," 2016.
- [29] Michael Rutherford, Seong K. Mun, Betty Levine, William C. Bennett, Kirk Smith, Phil Farmer, Jeremy Jarosz, Ulrike Wagner, Keyvan Farahani, and Fred Prior, "A dicom dataset for evaluation of medical image de-identification (pseudo-phi-dicom-data)," 2020.
- [30] Tong Tong and Menglei Li, "Abdominal or pelvic enhanced ct images within 10 days before surgery of 230 patients with stage ii colorectal cancer," 2022.
- [31] Blaine Rister, Kaushik Shivakumar, Tomomi Nobashi, and Daniel L. Rubin, "Ct-org: A dataset of ct volumes with multiple organ segmentations," 2019.
- [32] Afua A. Yorke, Gary C. McDonald, David Solis, and Thomas Guerrero, "Pelvic reference data," 2019.
- [33] Charles Roche, Ermelinda Bonaccio, and Joe Filippini, "The cancer genome atlas sarcoma collection (tcga-sarc)," 2016.
- [34] Sartaj Bhuvaji, Ankita Kadam, Prajakta Bhumkar, Sameer Dedge, and Swati Kanchan, "Brain tumor classification (mri)," 2020.
- [35] Zahra Mousavi Kouzehkanan, Sepehr Saghari, Sadjad Tavakoli, Peyman Rostami, Mohammadjavad Abaszadeh, Farzaneh Mirzadeh, Esmaeil Shahabi Sattisar, Maryam Gheidishahran, Fatemeh Gorgi, Saeed Mohammadi, et al., "A large dataset of white blood cells containing cell locations and types, along with segmented nuclei and cytoplasm," *Scientific reports*, vol. 12, no. 1, pp. 1123, 2022.
- [36] Angel Cruz-Roa, Ajay Basavanahally, Fabio González, Hannah Gilmore, Michael Feldman, Shridar Ganesan, Natalie Shih, John Tomaszewski, and Anant Madabhushi, "Automatic detection of invasive ductal carcinoma in whole slide images with convolutional neural networks," in *Medical Imaging 2014: Digital Pathology*. SPIE, 2014, vol. 9041, p. 904103.
- [37] Andrew Janowczyk and Anant Madabhushi, "Deep learning for digital pathology image analysis: A comprehensive tutorial with selected use cases," *Journal of pathology informatics*, vol. 7, no. 1, pp. 29, 2016.
- [38] Jakob Nikolas Kather, Niels Halama, and Alexander Marx, "100,000 histological images of human colorectal cancer and healthy tissue," *Zenodo10*, vol. 5281, 2018.
- [39] Marc Macenko, Marc Niethammer, James S Marron, David Borland, John T Woosley, Xiaojun Guan, Charles Schmitt, and Nancy E Thomas, "A method for normalizing histology slides for quantitative analysis," in *2009 IEEE international symposium on biomedical imaging: from nano to macro*. IEEE, 2009, pp. 1107–1110.
- [40] Muhammad EH Chowdhury, Tawsifur Rahman, Amith Khandakar, Rashid Mazhar, Muhammad Abdul Kadir, Zaid Bin Mahbub, Khandakar Reajul Islam, Muhammad Salman Khan, Atif Iqbal, Nasser Al Emadi, et al., "Can ai help in screening viral and covid-19 pneumonia?," *Ieee Access*, vol. 8, pp. 132665–132676, 2020.
- [41] Tawsifur Rahman, Amith Khandakar, Yazan Qiblawey, Anas Tahir, Serkan Kiranyaz, Saad Bin Abul Kashem, Mohammad Tariqul Islam, Somaya Al Maadeed, Susu M Zughaier, Muhammad Salman Khan, et al., "Exploring the effect of image enhancement techniques on covid-19 detection using chest x-ray images," *Computers in biology and medicine*, vol. 132, pp. 104319, 2021.
- [42] Walid Al-Dhabyani, Mohammed Gomaa, Hussien Khaled, and Aly Fahmy, "Dataset of breast ultrasound images," *Data in brief*, vol. 28, pp. 104863, 2020.
- [43] Olivia Cardozo, Verena Ojeda, Rodrigo Parra, Julio César Mello-Román, José Luis Vázquez Noguera, Miguel García-Torres, Federico Divina, Sebastian A Grillo, Cynthia Villalba, Jacques Facon, et al., "Dataset of fundus images for the diagnosis of ocular toxoplasmosis," *Data in Brief*, vol. 48, pp. 109056, 2023.